CHARACTERIZATION OF ALUMINA MICROSPHERES PRODUCED BY COMBUSTION TORCH REMELTING

N. SILIN[1], A. FERNANDEZ ZUVICH[2], A. SOLDATI[3] and A. BEVILACQUA[4]

[1] *Centro Atómico Bariloche – CNEA, CONICET, Av. Bustillo 9500, 8400 Bariloche, Argentina*
silin@cab.cnea.gov.ar
[2] *Centro Atómico Bariloche – CNEA, Av. Bustillo 9500, 8400 Bariloche, Argentina*
afz@cab.cnea.gov.ar
[3] *Centro Atómico Bariloche – CNEA, CONICET, Av. Bustillo 9500, 8400 Bariloche, Argentina*
asoldati@cab.cnea.gov.ar
[4] *Centro Atómico Bariloche – CNEA, Av. Bustillo 9500, 8400 Bariloche, Argentina*
bevi@cab.cnea.gov.ar

***Abstract*— The present work investigates the thermal treatment of alumina powder with a purpose built oxygen-Liquefied Petroleum Gas torch, pursuing a low-cost alumina microsphere production process. In this dry process, irregularly shaped alumina particles are re-melted, acquiring a spherical shape due to surface tension. Microspheres were produced starting from two different alumina powders, both having a granule size of approximately 80 µm. Two different starting materials with different porosity were tested. In both cases the resulting microspheres present similar surface texture and the predominant crystalline phase is α-alumina. Microspheres smaller than 42 µm show a dendritic morphology on the surface with minor presence of γ-alumina. In contrast, microspheres larger than 103 µm present a smoother surface with rhombohedral grains and no significant presence of γ-alumina.**

***Keywords*— SPHEROIDIZATION; FLAME; PRODUCTION; BEADS; AL2O3**

I. INTRODUCTION

Both, the industry and the academia have developed a wide spectrum of spherical particles for a broad range of applications. Even if we limit the spectrum to ceramic microspheres we can find a variety of production methods that result in microspheres with different diameters, densities and crystalline structure. It is possible to have great control over the characteristics of microspheres. Ray et al. produced alumina microspheres by sol-gel with densities close to 100% of the theoretical value, sizes between 4 and 30 µm and predominant phases being γ and δ (Ray et al., 1993). Chatterjee et al. studied how to variate the dimensions of the microspheres down to the micrometric scale while other researchers have obtained microspheres with variable density or porous structure (Chatterjee et al., 2000; Junqi et al., 2010). At the present a wide range of sizes, densities, microstructures and porosities can be produced, the largest limitation being the high cost of most processes, which greatly limits the spectrum of applications.

In general any process that involves the melting of alumina into droplets, results in the production of alumina microspheres (Luo and Wang, 2018). A simple and relatively inexpensive method to produce alumina microspheres in large volumes is therefore the thermal treatment of irregularly shaped alumina particles or aggregates. An early study performed by Plummer presents a device where particles in the order of 20 µm are melted in a hydrogen-oxygen torch to form droplets that are rapidly quenched (Plummer, 1958). He showed that the microspheres produced retained metastable δ and θ alumina phases, which could be converted to α alumina through calcination at 1180ºC. The effect of thermal treatment on the microstructure and crystallographic phases of alumina microspheres has been the subject to many research works as it can be linked to the mechanical characteristics of the resulting material (Dhakar et al., 2017).

Most recent works dealing with the production of alumina microspheres by thermal treatment use plasma torches. This method has the advantage of using a controlled atmosphere during the process, therefore attaining very high product purity and enabling medical applications. Plasma torches also produce violent temperature swings resulting in the retention of γ alumina (Chaturvedi et al., 2014) or even θ and δ alumina, depending on several process parameters such as the plasma torch power density (Peng et al., 2007). One downside of plasma torches is the limitation in the sizes of the microspheres that can be produced. Pershin et al. used a mixture of CO2–CH4 gases to increase the enthalpy of the plasma to obtain larger alumina microspheres, reaching a particle size of approximately 45 µm (Pershin et al., 2013). The microspheres obtained show a dendritic structure on the surface and are composed mainly of α and δ phases.

Another limitation of plasma processing is the low production throughput, due to the difficulty in scaling up plasma torches (Jang et al., 2012). To produce larger volumes of alumina microspheres, thermal processing

through combustion torches might be an attractive alternative. The possible application fields of alumina microspheres so produced will be dictated by their morphology, crystallography, porosity and purity. Some applications such as shot peening, bead blasting (Kajihara et al., 2018), grinding (Xiao et al., 2019) or as structural filler in composite materials (Agrawal and Satapathy, 2019; Ashwath and Xavior, 2018) are also very cost sensitive, while they require good mechanical properties. Even though combustion flames have been widely used to produce glass beads and microspheres, both at laboratory and industrial scales, there is very scarce information on alumina microsphere production in the open literature. Plummer presents perhaps one of the first and few works on alumina microsphere production by combustion torches (Plummer, 1958). More recently Jin et al. applied an oxygen-acetylene torch to produce 20 µm in diameter spherical silica as a low cost method (Jin et al., 2010). This is a relevant precedent as silica has a melting point close to the one of alumina, but a higher heat capacity.

In this work we focus in the characterization of alumina microspheres, with a diameter of approximately 80 µm, that were produced by means of a purpose made oxygen-Liquefied Petroleum Gas (LPG) burner. We explore their morphology, crystallography, and Carbon and Sulphur content as this information will enable to later evaluate the possible range of applications of the product. We have also used two different starting alumina powders, varying both in porosity and crystalline phases, but with similar granule size, to verify the influence of the starting materials on the properties of the final product.

II. MATERIALS AND METHODS

Microspheres were produced by thermally processing alumina powder in granules having a size similar to the intended final microsphere. A small, purpose built ejector is used to disperse and incorporate the powder into the carrier oxygen stream. A purpose built, surface-mixing combustion torch generates the flame and allows the carrier gas and particles to enter the flame through the center. A photograph of the flame and the main dimensions of the front plate of the surface mixing torch are shown in Fig. 1. It was observed that best spheroidization results were achieved using a slightly LPG rich mixture, probably due to the use of pure oxygen as carrier gas. The torch was operated with an LPG flow rate of 8 lpm, a primary oxygen flow rate of 24 lpm and a powder carrier oxygen flow rate of 1.5 lpm. The powder feed rate was kept at approximately 1 g/min. The particles travel a distance of approximately 150 mm in the flame (Fig. 1(a)) and the flying speed of the granules, as estimated from high speed video recording is approximately 15 m/s, giving an overall residence time in the order of 0.01 s.

The morphology of the starting materials and of the microspheres produced was observed with a Scanning Electron Microscope (SEM, Zeiss Crossbeam 340). The crystallographic phases present in the materials were evaluated by X-Ray Diffraction (XRD). XRD patterns were acquired with a Bruker D8 Advance instrument (CuKα radiation) equipped with a PSD detector (Lynx-Eye). Diffractograms were obtained in the 15°< 2θ <90° region, with a step size of 0.02°. The data was processed with the program X-Pert © (PANalytical, XpertHighScore Plus 2011).

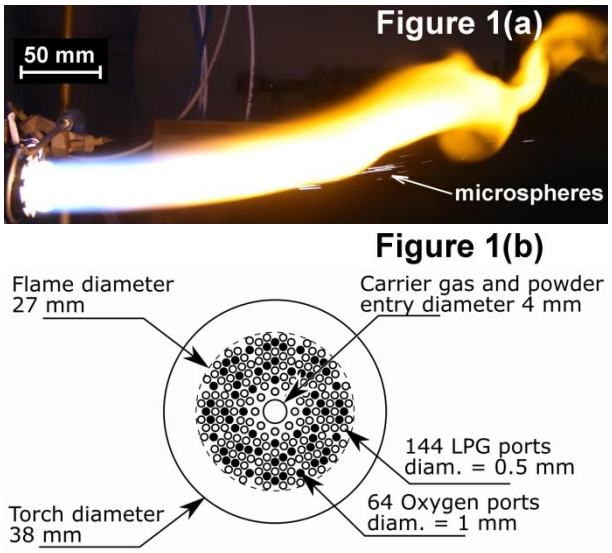

Figure 1: Processing setup. (a) Photograph of the combustion flame during operation. (b) Surface-mixing combustion torch.

To evaluate crystallographic differences as a function of microsphere size, we screened the microspheres with sieves, retaining the fraction larger than 103 µm and smaller than 43 µm, significantly larger and smaller than the bulk of the original sample respectively.

Textural characteristics of the samples were studied using a Micromeritics ASAP 2020 analyzer. N2 adsorption isotherms were collected at -196 ºC on 0.5 g of sample, after evacuation at 350 ºC overnight. Surface area was obtained applying the method of Brunauer, Emmett and Teller (BET method).

The content of Carbon and Sulphur was measured by means of a Leco CS230 Carbon and Sulphur Determinator.

III. RESULTS

The starting materials are two typical commercial alumina forms. In Fig. 2 we can see micrographs of the two materials, one (SP1) composed of granulated crystalline particles of Corundum (Anedra) , and another composed of granules with nanometric grain size (SP2) (Merck). Even though both materials are highly porous, SP1 has larger and better connected porosity, allowing gases to flow more easily, i.e. it shows higher permeability, while SP2 has a much finer structure which is expected to show lower permeability (Kozeny, 1927).

The general aspect of the microspheres produced from SP1 (µs_SP1) and from SP2 (µs_SP2) can be observed in Fig. 3. We could find very few particles that are fractured or have not been spheroidized. Micro-

spheres µs_SP2 are larger in size, which is also verified by the particle size analysis described below. Surface area obtained by the BET method for SP1, µs_SP1 and µs_SP2 resulted in values smaller than 1 m2/g. In contrast SP2 showed a value of 69 m2/g, indicating that it has a very fine interconnected porosity. This porosity is expected to produce higher gas retention during the spheroidization (Carman, 1997).

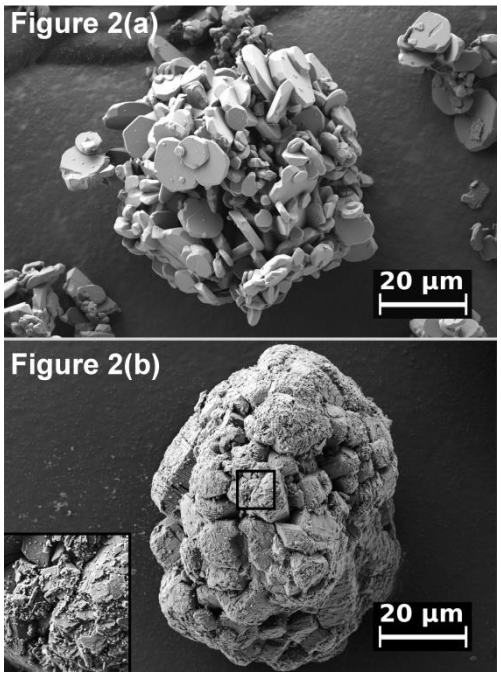

Figure 2: Micrographs of the starting material (a) SP1, (b) SP2.

The granule size distribution of the starting material and the size distribution of the microspheres were measured by means of a Mastersizer 3000 (Fig. 4). The size distribution of the microspheres was further verified by measuring the size of 300 individual microspheres from SEM images, for each starting material. The obtained microspheres are consistently smaller than the starting granules, this is a good sign as larger microspheres would indicate clustering or high porosity in the produced microspheres. The Dv50, of the starting materials SP1 and SP2 is 70 µm and 112 µm respectively while for the microspheres it is 60 µm and 82 µm respectively.

One distinctive feature of the produced microspheres is the occurrence of dendritic morphology on the surface, as can be observed in Fig. 3 (a) and (b). Only the largest microspheres showed a smoother surface with rhombohedral grains. This is a relevant feature as surface quality might affect the performance of the microspheres in certain applications. The occurrence of dendrites has been previously observed in microspheres produced by plasma torch (Pershin et al., 2013)(Solonenko et al., 2011).

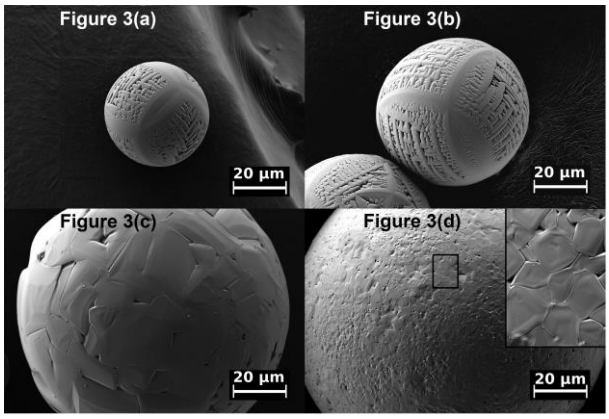

Figure 3: SEM images of individual alumina microspheres. (a) Smaller microspheres obtained from SP1 and (b) from SP2 showing a dendritic morphology. (c) Larger microspheres obtained from SP1 and (d) from SP2 showing a smoother surface with a rhombohedral grains.

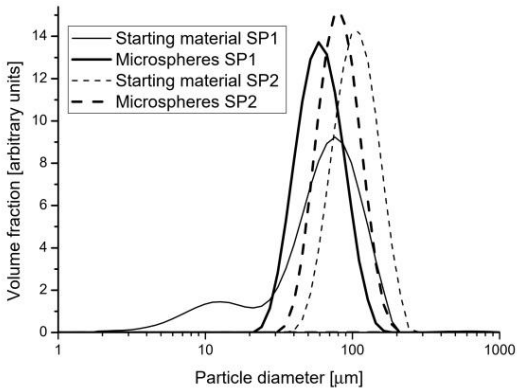

Figure 4: Granule size distribution of the starting materials and of the produced microspheres.

It is worth noting that the microspheres obtained in the present work have a clean surface. In contrast, microspheres produced by plasma torch processing show a surface covered with nanometric particles, as can be observed for instance in the work of (Peng et al., 2007). The cleaner surface might be due to the relatively low powder feed rate used in the present study and to the lower temperature achieved as compared to plasma torches, producing a low concentration of condensable vapors in the process gasses.

Figure 5 shows microspheres obtained from SP1 and SP2 that were included in epoxy resin and polished to unveil their internal microstructure. Microspheres show a rhombohedral microstructure. It can be observed that even though both microspheres show internal porosity, microspheres obtained from SP2 present a larger central void and a finer structure in the rest of the volume. This is in agreement with the finer structure of the starting material SP2 that makes it more difficult for gasses to migrate to the exterior (Solonenko, 2014). Measured densities are (3.4±0.2) g/cm^3 for µs_SP1 and (3.2±0.2) g/cm^3 for µs_SP2. In both cases it can be concluded that the whole granule underwent melting as no remains of

the original grain morphology can be observed and central voids are perfectly spherical.

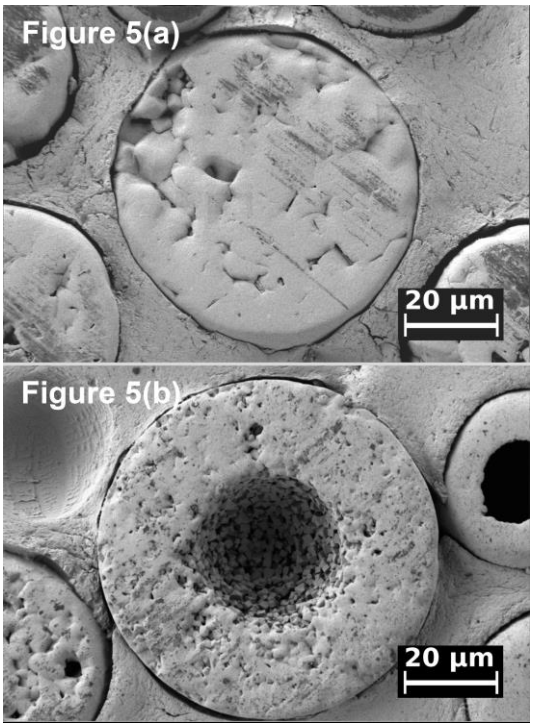

Figure 5: SEM images of alumina microspheres that were included in epoxy resin and polished to unveil their internal microstructure. (a) microspheres produced from SP1 and (b) from SP2.

In Fig. 6 we show the X-ray diffraction patterns for the starting materials SP1 and SP2 as well as the resulting microspheres µs_SP1 and µs_SP2, respectively. Following the guidelines of Feret et al. (Feret et al., 2000) to perform the analysis of the crystalline phases it was observed that only the starting materials differ significantly. Whereas SP1 shows a XRD diffractogram that closely matches that of the reference pattern 00-005-0712 for rhombohedral α alumina (Corundum) quantified as (97 ± 5) % rhombohedral phase according to reference pattern 01-075-1865, SP2 has a fuzzy diffractogram with peaks that match those of the reference pattern 00-010-0425 for cubic γ alumina quantified as (84 ± 5) % cubic and (16 ± 5) % rhombohedral phases according to reference patterns 01-077-0396 and 01-076-0144, respectively. After observations with SEM we can assume that this diffractogram is consistent with the material being formed by nanometric cubic γ alumina grains (Fig. 2). Further information can be found in the work of Wefers and Misra (Wefers and Misra, 1987). The resulting microspheres from both starting materials have very similar XRD, where the most notorious peaks at 2θ positions of 25.58º, 35.14º, 43.36º, 52.55º and 57.52º correspond to α alumina while some smaller peaks at 2θ positions of 31.93º and 45.86º correspond to γ alumina. Quantitatively µs_SP1 shows (93 ± 5) % rhombohedral and (7 ± 5) % orthorhombic phases according to reference patterns 01-074-1081 and 00-046-1215, respectively, and µs_SP2 shows (96 ± 5) % rhombohedral and (4 ± 5) % orthorhombic phases according to reference patterns 01-082-1399 and 00-046-1215, respectively.

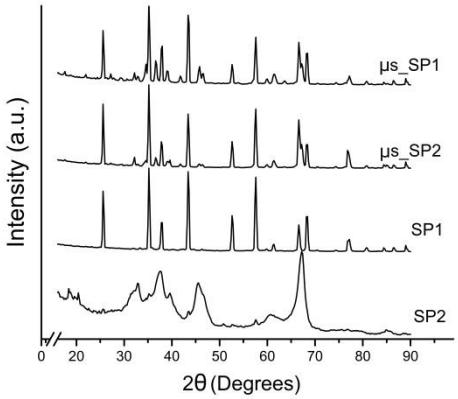

Figure 6: XRD spectra of the starting materials SP1 and SP2, and from the microspheres produced from both materials µs_SP1 and µs_SP2.

As we mentioned before, only the largest microspheres did not show a dendritic surface morphology, these microspheres have a superficial structure that reflects rhombohedral grains. From the microspheres produced from SP1 we have sieved apart the fraction smaller than 42 µm and the fraction larger than 103 µm and obtained the XRD spectra of each. The results are shown in Fig. 7 and it becomes clear that microspheres larger than 103 µm consist primarily of rhombohedral α alumina semi-quantitatively estimated as 95% while microspheres smaller than 42 µm also show intensity peaks corresponding to cubic γ alumina at 2θ of 31.93º and 45.86º semi-quantitatively estimated as 20%.

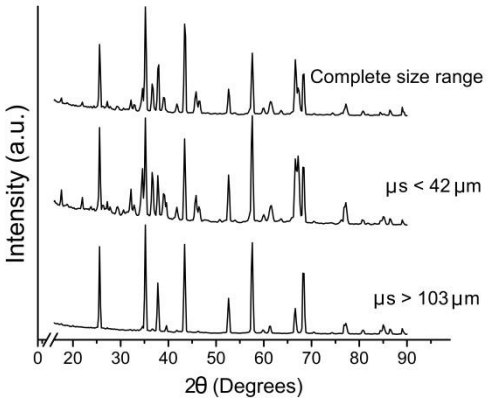

Figure 7: XRD spectra of the microspheres obtained from SP1, from the fraction of microspheres larger than 103 µm and from the fraction of microspheres smaller than 42 µm.

One concern with this processing method is that the resulting product might become contaminated with trace

elements from the combustion gases. A chemical composition analysis was done by means of the Leco CS230 Carbon and Sulphur Determinator. Results shown that only the starting material SP2 has a measurable content of Carbon and Sulphur before the thermal treatment, 0.13 g / 100 g Carbon content and 0.05g / 100 g Sulphur content. The starting material SP1 and the microspheres produced from both materials show a Carbon concentration of 0.03 g / 100 g and a Sulphur concentration lower than 0.006 g / 100 g, which is the minimum resolution of the determinator.

IV. DISCUSSION

It has been reported in the work of Sarjeant and Roy (Sarjeant and Roy, 1967) that, by means of rapid quenching, alumina can retain metastable phases. In processes like alumina molten spray coating, significant fractions of metastable phases of alumina are retained both using plasma spray (Iwamoto et al., 1977; Vetrivendan et al., 2017) or combustion flame spray (Aneziris et al., 2011). The presence of metastable phases, should decrease the slower the cooling process. It has been postulated by (McPherson, 1973) that larger microspheres attain a smaller degree of subcooling at the point of solidification initiation. This would also produce a slower solidification resulting in a more complete transformation of larger microspheres to α phase, as discussed by Das and Fulrath (Das and Fulrath, 1963). Meanwhile smaller microspheres, cooling faster, retain a larger proportion of metastable phases.

Also the surface morphology has been studied in depth for metal alloys in the context of welding technology. It has been established that for metal alloys, solidification morphology is significantly affected by the combination of temperature gradient in the liquid at the solidification boundary, and the solidification rate (Kou, 2003). It is apparent from the present results that similar trends may happen in the rapid solidification of alumina.

V. CONCLUSIONS

Spherical microspheres of alumina were produced by an oxygen-LPG combustion torch and characterized. Two different starting alumina powders were used, having different crystallographic characteristics and microstructures but composed of granules with similar overall size distribution. Irrespective of the starting alumina powder, most of the microspheres obtained show a dendritic morphology and are mostly composed of α alumina with a minor fraction of γ alumina. Only the largest microspheres show a smooth surface with a grain surface that reflects the rhombohedral microstructure. These microspheres also present complete conversion to stable α phase alumina. The main difference observed between the microspheres produced from different starting powders seems to be the final porosity and the existence of voids in the center of the microspheres. This difference can be attributed to the lower permeability of the starting material (SP2).

Differences in surface morphology as well as in crystallography are clearly correlated to particle size and consistent with differences in heating and cooling speeds.

ACKNOWLEDGEMENTS

The authors wish to express their recognition for the work of Gustavo Sepulveda, who made the combustion torch and other devices used in the present work, of Fernando Becker and Carolina Ayala who prepared the samples for SEM and XRD and of Silvina Pérez Fornells who helped with the acquisition of SEM images and participated in rich discussions.

REFERENCES

Agrawal, A., Satapathy, A., 2019. Thermal, mechanical, and dielectric properties of aluminium oxide and solid glass microsphere-reinforced epoxy composite for electronic packaging application. Polymer Composites 40, 2573–2581.

Aneziris, C.G., Gehre, P., Kratschmer, T., Berek, H., 2011. Thermal shock behavior of flame-sprayed free-standing coatings based on Al2O3 with TiO2- and ZrO2-additions. International Journal of Applied Ceramic Technology 8, 953–964.

Ashwath, P., Xavior, M.A., 2018. Effect of ceramic reinforcements on microwave sintered metal matrix composites. Materials and Manufacturing Processes 33, 7–12.

Carman, P.C., 1997. Fluid flow through granular beds. Chemical Engineering Research and Design 75, S32–S48.

Chatterjee, M., Naskar, M.K., Siladitya, B., Ganguli, D., 2000. Role of organic solvents and surface-active agents in the sol-emulsion-gel synthesis of spherical alumina powders. Journal of Materials Research 15, 176–185.

Chaturvedi, V., Ananthapadmanabhan, P.V., Chakravarthy, Y., Bhandari, S., Tiwari, N., Pragatheeswaran, A., Das, A.K., 2014. Thermal plasma spheroidization of aluminum oxide and characterization of the spheroidized alumina powder. Ceramics International 40, 8273–8279.

Das, A.R., Fulrath, R.M., 1963. Liquid-solid transformation kinetics in Al2O3.

Dhakar, B., Chatterjee, S., Sabiruddin, K., 2017. Phase stabilization of plasma-sprayed alumina coatings by spraying mechanically blended alumina–chromia powders. Materials and Manufacturing Processes 32, 355–364.

Feret, F.R., Roy, D., Boulanger, C., 2000. Determination of alpha and beta alumina in ceramic alumina by X-ray diffraction. Spectrochimica Acta Part B: Atomic Spectroscopy 55, 1051–1061.

Iwamoto, N., Makino, Y., Tanaka, K., 1977. Fundamental Considerations on Plasma Sprayed Ceramic Coating (Report II): Structural Study of Plasma Sprayed Al_2O_3. Transactions of JWRI 6, 267–271.

Jang, J., Takana, H., Park, S., Nishiyama, H., 2012. Advancement of in-flight alumina powder spheroidization process with water droplet injection using a small power DC-RF hybrid plasma flow system. Journal of thermal spray technology 21, 900–907.

Jin, H., Xu, L., Hou, S., 2010. Preparation of spherical silica powder by oxygen–acetylene flame spheroidization process. Journal of Materials Processing Technology 210, 81–84.

Junqi, L., Zuoli, H., Liying, G., Zhenfeng, Z., 2010. Synthesis and characterization of size-controlled TiO2 microspheres with wormhole mesoporous structure. Materials and Manufacturing Processes 25, 990–993.

Kajihara, Y., Tamura, Y., Kimura, F., Suzuki, G., Nakura, N., Yamaguchi, E., 2018. Joining strength dependence on molding conditions and surface textures in blast-assisted metal-polymer direct joining. CIRP Annals 67, 591–594.

Kou, S., 2003. Welding metallurgy. New Jersey, USA 431, 223–225.

Kozeny, J., 1927. Ueber kapillare leitung des wassers. Boden sitzungsberichte wiener akademie 136, 271–306.

Luo, Y., Wang, X., 2018. Morphology investigation of removal particles during laser cutting of Al2O3 ceramics based on vapor-to-melt ratio. Journal of Materials Processing Technology 255, 340–346.

McPherson, R., 1973. Formation of metastable phases in flame-and plasma-prepared alumina. Journal of Materials Science 8, 851–858.

Peng, H., Shikai, Y., Fangli, Y., Liuyang, B., Jinlin, L., Yunfa, C., 2007. Effect of plasma spheroidization process on the microstructure and crystallographic phases of silica, alumina and nickel particles. Plasma Science and Technology 9, 611.

Pershin, L., Mitrasinovic, A., Mostaghimi, J., 2013. Treatment of refractory powders by a novel, high enthalpy dc plasma. Journal of Physics D: Applied Physics 46, 224019.

Plummer, M., 1958. The formation of metastable aluminas at high temperatures. Journal of Applied Chemistry 8, 35–44.

Ray, J., Chatterjee, M., Ganguli, D., 1993. Sol-gel-derived alumina microspheres. Journal of materials science letters 12, 1755–1757.

Sarjeant, P.T., Roy, R., 1967. New glassy and polymorphic oxide phases using rapid quenching techniques. Journal of the American Ceramic Society 50, 500–503.

Solonenko, O.P., 2014. Criterion conditions for the formation of hollow microspheres from plasma-treated agglomerated particles. Thermophysics and Aeromechanics 21, 735–746.

Solonenko, O.P., Gulyaev, I.P., Smirnov, A.V., 2011. Thermal plasma processes for production of hollow spherical powders: Theory and experiment. Journal of Thermal Science and Technology 6, 219–234.

Vetrivendan, E., Thendral, G., Shankar, A.R., Mallika, C., Kamachi Mudali, U., 2017. Aluminum phosphate sealing to improve insulation resistance of plasma-sprayed alumina coating. Materials and Manufacturing Processes 32, 1435–1441.

Wefers, K. and Misra, C., 1987. Oxides and hydroxides of aluminum (Vol. 19, pp. 1-92). Pittsburgh: Alcoa Laboratories.

Xiao, C., Chen, C., Wang, H., Chen, L., Jiang, L., Yu, B., Qian, L., 2019. Effect of counter-surface chemistry on defect-free material removal of monocrystalline silicon. Wear 426, 1233–1239.